Engineering Structures 161 (2018) 41–54

Contents lists available at ScienceDirect

Engineering Structures

journal homepage: www.elsevier.com/locate/engstruct

Strut-and-tie models for deteriorated reinforced concrete half-joints

Pieter Desnerck[a,b,*], Janet M. Lees[b], Chris T. Morley[b]

[a] Department of Civil and Environmental Engineering, Brunel University London, Kingston Lane, UB8 3PH Uxbridge, UK
[b] Department of Engineering, University of Cambridge, UK

ARTICLE INFO

Keywords:
Strut-and-tie modelling
Corrosion
Deterioration
Synergistic effects
Reinforced concrete half-joints
Assessment

ABSTRACT

A reinforced concrete half-joint bridge consists of suspended span dapped-end beams or a full-width deck supported on the nibs of abutments or adjacent beams. The design of their disturbed regions is traditionally performed by means of strut-and-tie modelling. The design provisions found in standards and codes can be used for the assessment of existing structures with minor adjustments. However, current documents provide limited guidance on the incorporation of deterioration aspects such as corrosion, insufficient anchorage lengths, and crack formation.

Experiments performed on 12 half-joint beams demonstrated the effects of single defects, but synergistic effects were also found to exist and might lead to much higher reductions than expected from the sum of individual defects. These results were compared to different strut-and-tie models (STMs) and the application of STMs to achieve the highest lower bound estimate of the load carrying capacity is discussed.

For the beams studied in the current work, the predictions based on codes and standards, combined with appropriate methods to incorporate deterioration effects, led to safe load bearing capacity estimates. However, the developed STMs seem to be, in some instances, unable to pick up alternative load paths that develop as soon as the capacity of a certain tie is reached. Hence the actual capacities might be higher than what is obtained from the STM calculations.

1. Introduction

With increasing traffic volumes and load demands in an era of limited resources, there is a pressing need for the accurate strength assessment of aging infrastructure. When assessing the load carrying capacity of existing bridges, the influence of factors including deterioration and previous repair works are often disregarded since current code provisions or guidelines do not provide sufficient guidance. However, the de la Concorde Overpass collapse in 2006 [1], killing 5 people, emphasises the importance of proper inspections, maintenance, and adequate assessment techniques.

Reinforced concrete half-joints, such as de la Concorde Overpass, provide specific challenges with respect to their assessment. A half-joint bridge consists of suspended span dapped-end beams or a full-width deck supported on the nibs of abutments or adjacent beams (Fig. 1). Advantages of this type of bridge detailing are the suitability for precast construction [2] and a reduced construction depth with a level running surface along the bridge deck and the support spans. Disadvantages are the vulnerability of the structures to deterioration at the nib due to seepage of chloride-rich water through the expansion joints and the existence of large regions that are not easily accessible for inspection or repair.

Common issues raised during half-joint bridge assessments are [3]:

- Deterioration of the concrete and/or reinforcement
- Inconsistencies between the as-built and as-designed internal steel reinforcement
- Non-compliance of half-joints with current code provisions

Deterioration processes, such as carbonation, chloride ingress, and freeze-thaw cycles, mean that the mechanical properties of the concrete and steel will alter over the lifetime of a reinforced concrete half-joint. The extent to which these processes affect the compressive strength, tensile strength and modulus of elasticity of the concrete can be significant [4].

During the design process, the reinforcement detailing can be carefully considered and specified, but in practice, the execution might prove to be difficult due to dense reinforcement cages or a lack of accessibility to certain regions within a specific half-joint geometry. These alterations might have a significant impact on the load carrying capacity of a structure and inconsistencies should be carefully analysed during the assessment. The misplacement of some of the reinforcing

* Corresponding author at: Department of Civil and Environmental Engineering, Brunel University London, Kingston Lane, UB8 3PH Uxbridge, UK.
E-mail address: Pieter.Desnerck@brunel.ac.uk (P. Desnerck).

https://doi.org/10.1016/j.engstruct.2018.01.013
Received 10 February 2017; Received in revised form 31 December 2017; Accepted 5 January 2018
Available online 02 February 2018

Nomenclature

Abbreviations and notations

α	residual bond factor (range of 0.15–0.40) [–]
α_s	angle between compressive strut and adjoining tension tie [–]
α_{cr}	bond reduction factor [–]
β	bar type coefficient (0.70 in case of deformed bars in tension) [–]
ε_s	tensile strain in concrete in direction of tension tie [–]
γ_{mb}	partial safety factor ranging between 1.25 and 1.4 [–]
λ	ratio of actual to provided bond length [–]
ν	reduction factor [–]
$\sigma_{c,st}$	concrete compressive stress in strut [MPa]
$\sigma_{s,st}$	steel compressive stress in strut reinforcement [MPa]
$\sigma_{s,tie}$	steel tensile stress in tie reinforcement [MPa]
$A_{c,st}$	effective concrete area of the strut [mm^2]
$A_{s,st}$	area of provided compressive reinforcement along strut [mm^2]
$A_{s,tie}$	area of provided tensile reinforcement along tie [mm^2]
A_{tr}	area of transverse reinforcement [mm^2]
D_0	original reinforcing bar diameter [mm]
d_b	reinforcement bar diameter [mm]
d_p	depth of pit corrosion [mm]
e	distance between the bearing plate and the reinforcing bar [mm]
f_{bd}	design bond strength assuming perfect bond conditions [MPa]
$f_{bd,red}$	reduced bond strength [MPa]
f_c'	concrete compressive strength [MPa]
f_{cd}	design concrete compressive strength [MPa]
f_{ck}	characteristic concrete compressive strength [MPa]
$f_{c,u}$	allowable concrete compressive stress [MPa]
f_n	lateral pressure [MPa]
f_s	steel stress at critical section [MPa]
f_y	yield stress of reinforcing steel [MPa]
f_{yd}	design yield stress of reinforcing steel [MPa]
$F_{n,st}$	bar force in a strut [N]
$F_{n,tie}$	bar force in a tie [N]
F_{ult}	ultimate failure load of half-joint [N]
$F_{ult,\ exp}$	experimentally obtained ultimate failure load of half-joint [N]
$F_{ult,\ STM}$	ultimate failure load of half-joint according to STM [N]
l_a	actual provided anchorage length of reinforcing bar [mm]
l_d	anchorage length of reinforcing bar [mm]
STM	strut-and-tie method]
s	spacing of reinforcing bars [mm]
t	depth of the strut [mm]
w	width of the strut [mm]
x_b, x_y	dimension of remaining cross-sectional area after corrosion [mm]
x_c, x_c	dimension of pitting corrosion [mm]

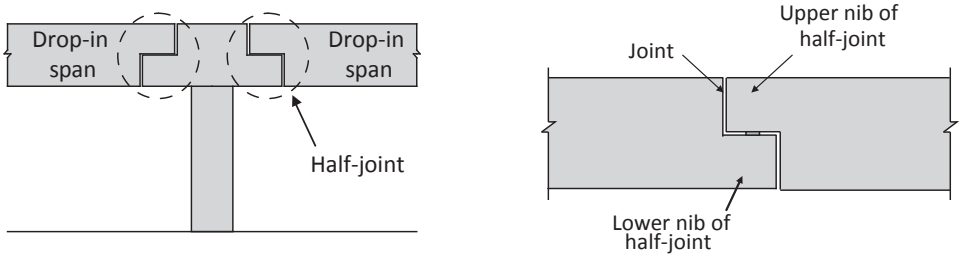

Fig. 1. Half-joint principle for reinforced concrete bridges.

bars was noted in the investigations into the de La Concorde Overpass collapse [5].

Code provisions have changed over the last few decades. Back in the 1960s and 1970s, the shear provisions, for example, were typically less stringent than they are in current codes. In some cases, minimum shear reinforcement ratios were not required [6] and, hence, older half-joints being assessed today might fail the assessment by default as they lack the minimum amount of shear links. Mitchell et al. [7] compared anchorage requirements for half-joints provided by historical and current versions of the PCI Handbook [8]. They concluded that there were cases where the older design guidance underestimated the need for anchorage measures and might provide insufficient protection against shear failure.

Hence, deterioration, inconsistencies and non-compliance with current codes can all create concerns when performing assessments. IAN 53/04 'Concrete Half-Joint Deck Structures' [9] states that assessors should use their engineering judgement to take into account the deteriorated state of the half-joint during capacity checks, including likely reinforcement section loss and any delamination of the concrete cover. BA 39/93 [10] on the 'Assessment of reinforced concrete half-joints' provides a method to evaluate crack widths (in the serviceability limit state) and emphasises the importance of accounting for corrosion effects in the calculations of the ultimate load capacity. In addition, IAN 53/04 specifically mentions the use of strut-and-tie methods (STM) to assess the remaining load carrying capacity of reinforced concrete half-joints. However, no specific guidance is provided on how to account for certain defects detected during inspections. The way in which deterioration and inadequate anchorage conditions should be dealt with remains unknown.

This paper summarizes the basis of the STM for assessment and STM provisions available in selected design codes. An experimental program exploring the impact of reinforcement layout, anchorage and concrete cracking on the structural capacity of half-joints is briefly discussed, after which the accuracy and validity of the current STM provisions are evaluated in the context of the experimental program.

2. Strut-and-tie method

The application of strut-and-tie methods for the assessment of reinforced concrete half-joints, differs from how STMs would be used in the design of new construction. Assessors are no longer able to design and place tensile reinforcement freely, but have to comply with the provided reinforcement layout of the structure under assessment. Other design options, such as the selection of the preferred concrete quality and strength, are also no longer available. Nevertheless, the use of a STM for assessment shows significant similarities to an STM design process. A typical STM design process can be split up into 3 main phases:

- Step 1: Defining the B- and D-regions

- Step 2: Development of a strut-and-tie model
- Step 3: Design of individual STM members

Each of these phases is discussed below, with emphasis on the half-joint specific aspects. In Section 3, the modifications when applying STMs to the assessment of existing reinforced concrete half-joints will be discussed in more detail.

2.1. Defining B- and D-regions

When designing reinforced concrete half-joints, the half-joint beams can be divided into B- and D-regions [11]. B-regions are those zones where the hypothesis of Bernoulli holds, whereas D-regions are areas of discontinuities in which the hypothesis is no longer valid. B-regions are usually assessed using 'normal' beam theory, while for D-regions STM methods can be used [12].

In order to identify the extent of a D-region, the St.-Venant's principle can be applied [13]. For half-joints, it is generally accepted [11,13–15] that the D-region extends into the full-depth section of the beam over a distance beyond the nib that is equal to the depth of the beam itself, as illustrated in Fig. 2.

Once the D-region has been identified, the bending moments, shear forces, and axial forces can be determined at the B-region/D-region interface.

2.2. Development of a strut-and-tie model

A strut-and-tie model consists of 3 main components: struts, ties, and nodes. The struts carry the compressive forces, and the ties are the tension members in the model. Nodes, or nodal areas, represent the points where the struts and ties meet [16].

For a given half-joint, a strut-and-tie model is not unique. The STM only requires that equilibrium and the yield criteria are satisfied and does not require strain compatibility. It is a lower bound plasticity method [11]. Hence, numerous strut-and-tie models can be mapped on to a specific half-joint design, as long as the external applied loads and reaction forces are in equilibrium with the assumed distribution of internal forces and the stresses developed in the struts, ties and nodes are within acceptable limits.

Several methods have been developed to identify possible strut-and-tie models, these are all based on elastic solutions [13]. With respect to half-joints, the most commonly used STMs can be grouped into one of three categories (see Fig. 3) that depend on the reinforcement layout. These are diagonal, orthogonal or combination models. In Europe, a diagonal reinforcement bar is often used to transfer (part of) the applied load from the nib to the full-depth section of the beam, leading to e.g. a diagonal strut-and-tie model (Fig. 3a) [17]. An approach more common in the US, however, is to provide a substantial amount of longitudinal reinforcement in the nib that extends sufficiently far into the full-depth section in conjunction with a reasonable amount of transverse steel in the full depth beam. This leads to orthogonal strut-and-tie models (Fig. 3b–d) [7,13,18]. More complex 'combination type' strut-and-tie models have been proposed for half-joints with diagonal bars [19–21] e.g. as shown in Fig. 3e.

Based on the reinforcement layout of the assessed half-joint structure, the engineer has to select a model where the tension ties line up with the reinforcement bars as closely as possible. A compressive strut can be freely placed as long as the angle between the strut and ties is within reasonable limits and the integrity of the concrete at that location is guaranteed. The chosen angle should be large enough to avoid strain incompatibilities. Several codes and guidelines suggest a minimum angle, such as 25° in ACI318 [22]. Furthermore, ACI318 allows ties to cross, but states that struts should only intersect or overlap at nodes. In Eurocode 2 [16] no explicit minimum value of the angle between the struts and ties is stipulated although 10% higher concrete stresses are allowed for angles above 55°. AASHTO, on the other hand, penalises the allowable concrete stress in struts at small angles [23].

2.3. Design of individual STM members

Once the forces in the different members of a particular strut-and-tie model have been determined, the allowable stresses in the individual members need to be verified. The stresses in all members should not exceed the allowable stresses under the applied (factored) load, in order to deem the half-joint to be safe.

2.3.1. Struts

The concrete compressive stress in the strut $\sigma_{c,st}$, can be calculated from:

$$F_{n,st} = \sigma_{c,st} A_{c,st} + \sigma_{s,st} A_{s,st} \tag{1}$$

where $F_{n,st}$ is the bar force in the strut obtained from the static truss analysis, $A_{c,st}$ is the effective concrete area of the strut, $A_{s,st}$ is the area of provided compression reinforcement along the strut, and $\sigma_{s,st}$ is the compressive stress in the reinforcement at the given strut force. This stress can be taken to be equal to the design yield stress of the reinforcing steel, f_{yd}, when the yield strength is reached.

The effective concrete area of the strut $A_{c,st}$ is determined by the width of the strut, w, and the depth t of the strut. The depth t can be taken as equal to the thickness of the specimen according to Eurocode 2 [16] and ACI 318 [22] unless the supports are narrower in which case the width of the strut should be taken to be equal to the width of the support for struts originating at the support. AASHTO [23] applies a more conservative approach for struts that are anchored by reinforcement. The effective concrete area of the strut in such cases has a width of 6 bar diameters (or 8 as suggested by Mitchell et al. [24]) from the anchoring bars (Fig. 4).

The applied concrete compressive stress in the strut $\sigma_{c,st}$ should not exceed the allowable concrete stress $f_{c,u}$. This allowable stress, also referred to as effective stress or limiting compressive stress, has been the subject of much debate, but is generally assumed to be a fraction (less than or equal to 1) of the concrete compressive strength f_c':

$$f_{c,u} = \upsilon f_c' \tag{2}$$

The factor ν takes into account the effect of concrete cracking and tensile strains transverse to the strut. Table 1 provides an overview of allowable stresses suggested by several researchers and found in code provisions.

As mentioned earlier, the AASHTO provisions take into account the angle α_s between the compressive strut and the adjoining tension ties in the determination of $f_{c,u}$:

$$f_{c,u} = \frac{f_c'}{0.8 + 170\varepsilon_1} \leqslant 0.85 f_c' \tag{3}$$

for which:

$$\varepsilon_1 = \varepsilon_s + (\varepsilon_s + 0.002) cot^2 \alpha_s \tag{4}$$

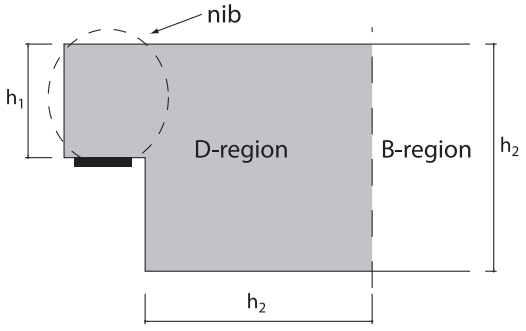

Fig. 2. B- and D-region for half-joint specimen.

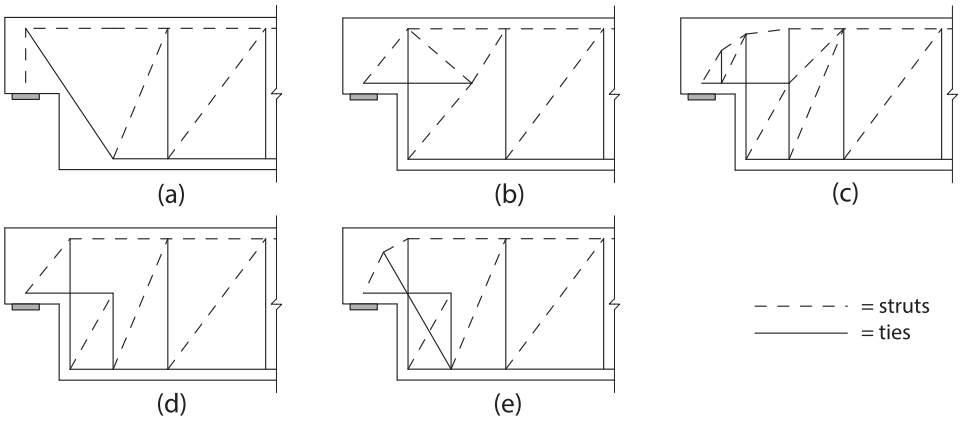

Fig. 3. Common strut-and-tie models for reinforced half-joints: (a) diagonal model, (b), (c) and (d) orthogonal models, and (e) combination type model.

where ε_s is the tensile strain in the concrete in the direction of the tension tie. In this way, even struts with very small angles can be taken into account, although their contribution will be small as can be seen in Eqs. (3) and (4).

2.3.2. Ties

The stress induced in a reinforcing tie of a reinforced concrete half-joint, $\sigma_{s,tie}$, can be calculated from:

$$F_{n,tie} = \sigma_{s,tie} A_{s,tie} \tag{5}$$

where $F_{n,tie}$ is the bar force in the tie obtained from the static truss analysis and $A_{s,tie}$ is the area of the provided tensile reinforcement. The induced stress $\sigma_{s,tie}$ is limited to the reinforcement design yield stress f_{yd}. Reference is made to fib Bulletin 45 [11] for guidance on incorporating the effect of tendons in pre-/post-tensioned elements.

According to Yun and Ramirez [27], concrete ties can be used in cases where steel reinforcement cannot be, or is not, provided. They suggest that the effective tensile stress level of a concrete tie can be taken as the smallest of the concrete rupture modulus or the tension failure stress of two-dimensional plain concrete under biaxial compression-tension loading which is approximately 0.1 f_c' [28]. However, concerns can be raised over this approach given the brittle nature of concrete tensile failure and the fact that the concrete tensile capacity can reduce over time (e.g. due to shrinkage, creep or corrosion cracking). In light of these concerns, in the current work concrete ties will not be used.

2.3.3. Nodes

A multi-directional stress state exists in nodes, where compressive struts and tension ties intersect. The strength of a node is dependent on the tensile straining (due to the tension ties), the confinement provided by compressive struts and the transverse reinforcement [29]. Four types of nodal conditions can be identified (Fig. 5). CCC or TTT type nodes are fairly rare in half-joint strut-and-tie models as most nodes are of the CCT or CTT type (Fig. 3). In several nodes of, e.g. the combination-type half-joint, more than 3 bars are joined. But, based on the modified hydrostatic approach, these can be converted to a series of closely linked 3 bar nodes as will be discussed later.

The allowable compressive stress in a node is determined by applying a reduction factor to the compressive strength of the material. Table 2 summarizes the proposed allowable nodal stresses as found in the selected literature and code provisions.

It is common practice to apply the classic method of hydrostatic node construction for the assessment of nodal zones [11]. For nodes where more than three members intersect, a modified hydrostatic approach as proposed by Schlaich and Anagnostou [30] can be taken (Fig. 6) to maintain a set of concurrent forces.

An important aspect of nodal zones is the anchorage check for the tension ties. Reinforcing bars need to be anchored properly to allow ties to develop their full capacity. Codes [22,23,31] generally agree that the anchorage length of a tie can be taken from the point where the resultant tension tie force enters the extended nodal zone, as illustrated in Fig. 7.

Tension ties in CCT and CTT nodes experience lateral pressure from the compressive strut. Therefore, Bergmeister et al. [32] suggest that the confinement action due to the lateral pressure reduces the required development length l_d. Based on test results, they suggested the following expression for l_d:

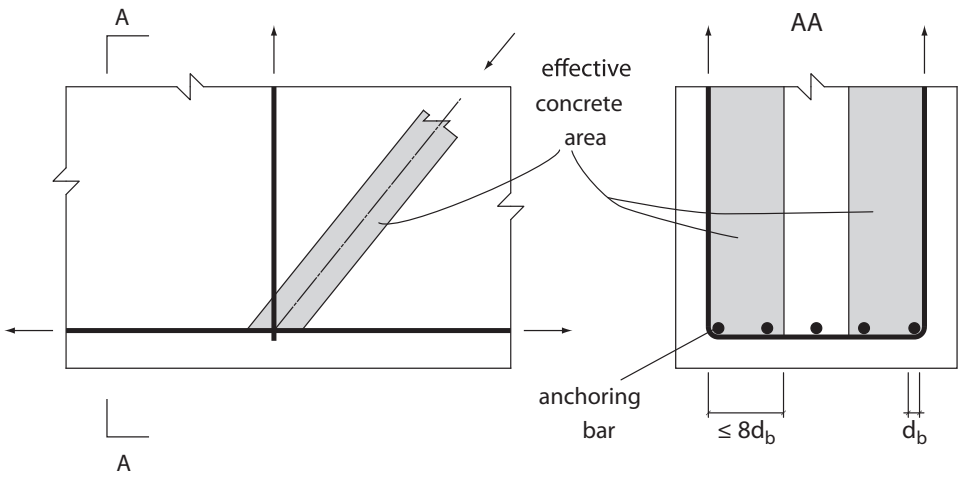

Fig. 4. Strut width according to AASHTO of a strut anchored by reinforcement.

Table 1
Allowable stress levels in concrete struts.

Allowable stress level	Concrete strut	Proposed by
0.80 f_c'	Undisturbed and uniaxial state of compressive stress that may exist for prismatic struts	Schlaich et al. [13]
0.68 f_c'	Tensile strain and/or reinforcement perpendicular to the axis of the strut may cause cracking parallel to the strut with normal crack width	
0.51 f_c'	Tensile strain causing skewed cracks and/or reinforcement at skew angles to the struts' axis	
0.34 f_c'	For skew cracks with extraordinary crack widths. Skew cracks would be expected if modelling of the struts departed significantly from the theory of elasticity's flow of internal forces	
0.85 f_c'	Moderately confined diagonal struts going directly from point load to support with shear span to depth ratio less than 2.0	Alshegeir [25]
0.75 f_c'	Struts forming arch mechanism	
0.50 f_c'	Arch members in pre-stressed beams and fan compression members	
0.95 f_c'	Undisturbed and highly stressed compression struts	
1.00 ν_2 $f_c'^{*}$	Uncracked uniaxially stressed struts or fields	MacGregor [26]
0.80 ν_2 $f_c'^{*}$	Struts cracked longitudinally in bulging compression fields without transverse reinforcement	
0.65 ν_2 $f_c'^{*}$	Struts cracked longitudinally in bulging compression fields with transverse reinforcement	
0.60 ν_2 $f_c'^{*}$	Struts in cracked zone with transverse tension from transverse reinforcement	
0.30 ν_2 $f_c'^{*}$	Severely cracked webs of slender beams with $\theta = 30^\circ$	
0.55 ν_2 $f_c'^{*}$	Severely cracked webs of slender beams with $\theta = 45^\circ$	
0.85 f_c'	Struts with uniform cross-sectional area along length	ACI 318 [22]
0.64 f_c'	Struts located in a region of a member where the width of the compressed concrete at mid-length can spread laterally (bottle-shaped struts) and with transverse reinforcement	
0.51 f_c'	Struts located in a region of a member where the width of the compressed concrete at mid-length can spread laterally (bottle-shaped struts) and without transverse reinforcement	
0.34 f_c'	Struts located in tension members or the tension zones of members	
0.51 f_c'	All other cases	
1.00 f_{cd} **	Compressive struts without tensile stresses in transverse direction	Eurocode 2 [16]
0.60 ν' f_{cd} **	Compressive struts with tensile stresses in transverse direction	
min ($f_c'/(0.8 + 170\varepsilon_1)$; 0.85 f_c')	Compressive strut at an angle with adjoining tension tie	AASHTO [23]

* With $\nu_2 = 0.5 + 1.25/\sqrt{(f_c')}$.
** With f_{cd} taken as the design concrete compressive strength and $\nu' = 1\text{-}f_{ck}/250$, f_{ck} the characteristic concrete compressive strength.

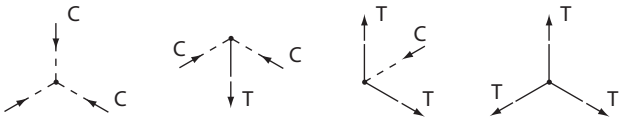

Fig. 5. Different types of nodes: CCC, CCT, CTT and TTT.

$$l_d = \frac{d_b\left[(3f_s/f_c'^{1/2}) - 50\right]}{1.2 + 3c/d_b + A + B} \tag{6}$$

with

$$A = (A_{tr}f_y)/(3.4sd_b) \leqslant 3.0 \tag{7}$$

$$B = f_n^{1/2}(2.4 - e^2/58000) \leqslant 6.0 \tag{8}$$

where d_b is the bar diameter, A_{tr} is the area of transverse reinforcement (normal to the plane of splitting through the anchored bars [33]), f_s is the steel stress at the critical section, e is the distance between the bearing plate and the reinforcing bar, f_n is the lateral pressure, and s is the spacing of the bars. The equation takes into account the lateral pressure up to a distance of $e = 350$ mm.

3. Use of Strut-and-Tie methods for the assessment of RC Half-Joints

The design principles and guidelines discussed in Section 2, can be

Table 2
Allowable stress levels in nodal zones.

Allowable stress level	Nodal zone	Proposed by
0.85 f_c'	CCC nodes	Schlaich et al. [13]
0.68 f_c'	Nodes where reinforcement is anchored in or crossing the node	
1.00 ν_2 $f_c'^{*}$	Nodes bounded by compressive struts and bearing areas	
0.85 ν_2 $f_c'^{*}$	Nodes anchoring one tension tie	MacGregor [26]
0.70 ν_2 $f_c'^{*}$	Nodes anchoring tension ties in more than one direction	
0.85 ϕ $f_c'^{**}$	Nodal zones bounded by compressive struts and bearing areas	AASHTO [23]
0.75 ϕ $f_c'^{**}$	Nodal zones anchoring one-direction tension tie	
0.65 ϕ $f_c'^{**}$	Nodal zones anchoring tension ties in more than one direction	
0.85 f_c'	Nodal zone bounded by struts, bearing areas, or both	
0.68 f_c'	Nodal zones anchoring one tie	ACI 318 [22]
0.51 f_c'	Nodal zones anchoring two or more ties	
ν' f_{cd} ***	Compression nodes where no ties are anchored at the node	Eurocode 2 [16]
0.85 ν' f_{cd} ***	Compression - tension nodes with anchored ties provided in one direction	
0.75 ν' f_{cd} ***	Compression - tension nodes with anchored ties provided in more than one direction	

* With $\nu_2 = 0.5 + 1.25/\sqrt{(f_c')}$.
** With ϕ being a capacity reduction factor for bearing (taken as 0.70 in ACI318-14 [22]).
*** Where f_{cd} is the design concrete compressive strength and $\nu' = 1\text{-}f_{ck}/250$.

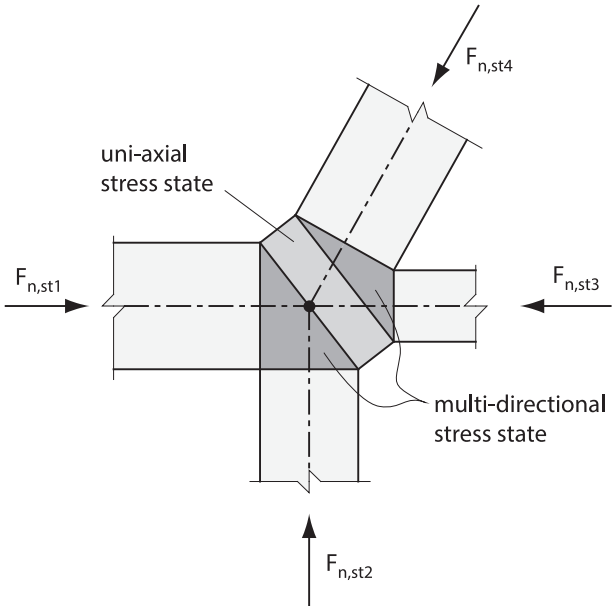

Fig. 6. Example of a modified hydrostatic node.

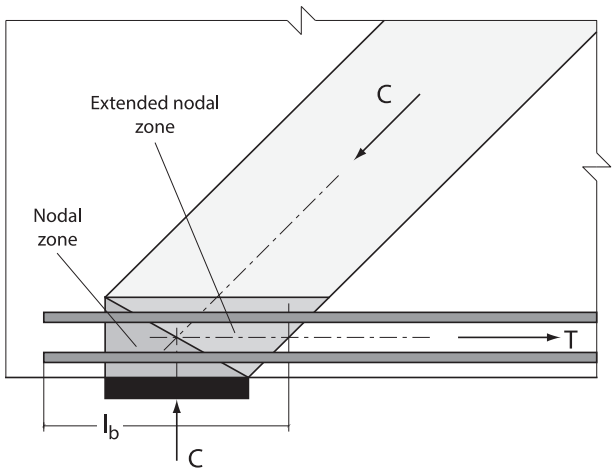

Fig. 7. Anchorage length of a tension tie.

used as the basis for a STM assessment process for existing reinforced concrete half-joints.

Bridge inspection reports can provide information about the integrity of the concrete and inform the potential location of struts. Existing crack patterns can also be used to identify the principal tensile and compressive stress directions at certain points in the half-joint, and hence the potential orientation and location of compressive struts.

The entire process in itself can become iterative. The calculation of the stresses in individual members in a strut-and-tie model might indicate that the allowable stresses have been exceeded or the reinforcement detailing provides insufficient anchorage. In such cases, the width of the struts can be adjusted (if the physical dimensions of the specimen allow) or the forces in the bars can be limited to reduce the demand on the anchorage. In this way, an iterative process is initiated. When additional iteration steps and corresponding adjustments no longer lead to an increase in load carrying capacity, the process can be stopped. The maximum load, carried by the STM, that was in compliance with the equilibrium requirements and yield analysis, and that does not lead to stresses exceeding the allowable levels, can be considered to be the load carrying capacity of the assessed half-joint.

However, limited knowledge and guidance is available with respect to the incorporation of defects, deterioration and/or construction errors in the assessment of reinforced concrete half-joints. When corrosion is detected BA38/98 [34] can be used, whereas for insufficient anchorage, Clark [35] has published recommendations.

3.1. Corrosion of tension ties

One of the most commonly detected deterioration outcomes in reinforced concrete half-joints is the corrosion of (part of) the steel reinforcing bars. According to guidance published by the UK Highways Agency (BA 51/95 [36]), general corrosion (over an extensive length of the rebar) should be taken into account by assuming the strength loss of the bar is proportional to the section loss (Fig. 8(a)) [36]. The remaining bar cross-sectional area can be taken as $\pi \cdot x_b \cdot y_b/4$ where x_b and y_b are measured in perpendicular directions and either x_b or y_b is the minimum width (Fig. 8(b)) when corrosion is detected mostly on one side of the rebar. BA38/98 [34] states that for local corrosion (e.g. pitting corrosion), the sectional loss can be accounted for in a similar way to general corrosion. The width x_c and depth y_c of the pitting corrosion are measured (Fig. 8(c) and (d)) and the total cross-sectional area is reduced by $x_c \cdot y_c$. For more irregular boundaries of damage, as shown in Fig. 8(e), an approximation of the un-corroded cross-sectional area can be made based on the net cross-sectional area.

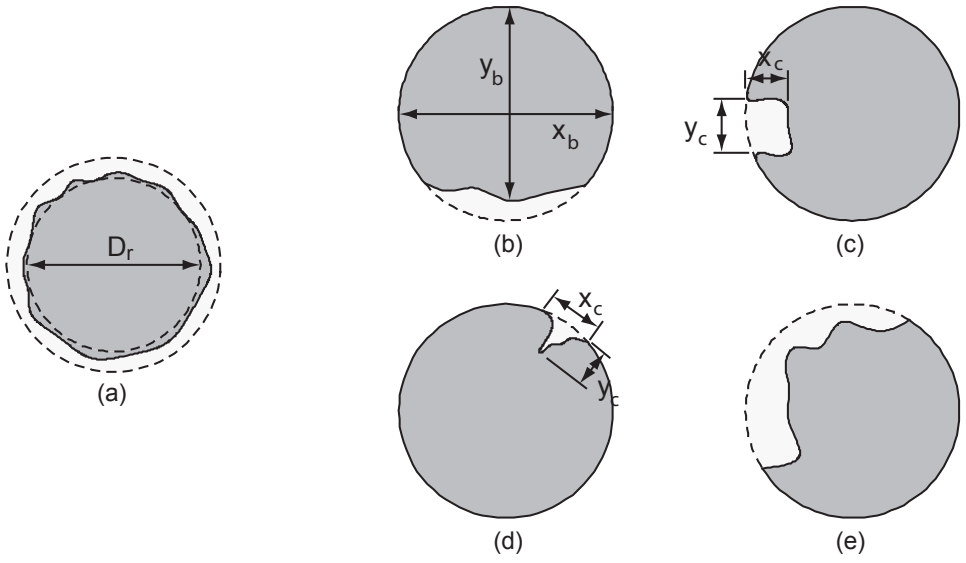

Fig. 8. Residual steel cross-section according to BA38/98 (based on [34]).

Other sources have suggested that the effect of pitting corrosion should be dealt with in a more conservative way (Fig. 9). Rodriguez et al. [37,39] suggest that the residual cross-sectional area of the corroding steel bar should be limited to a circular cross-section which fits below the maximum pit depth d_p (see Fig. 9a), although several researchers, including Harnisch [40], have shown this approach to be highly conservative. Val et al. [38] developed a dome-shaped corrosion pit model as shown in Fig. 9(b), which was later extended by Darmawan [41].

In all these cases, although the steel corrosion is considered to reduce the cross-sectional area, the steel properties are assumed not to be affected. Zhu and Francois [42] tested reinforcing bars with corrosion levels up to 50% and confirmed that, if the cross-sectional area loss is taken into account, the yield strength and rupture strength of the bars are not greatly affected by corrosion.

One important aspect to remember is that the STM is based on the lower bound theorem of plasticity and hence is only valid when adequate ductility can develop within the structure. Sufficient ductility of the concrete should be confirmed and a check of the reinforcing steel quality during the assessment (regardless of its corroded state) is advised.

3.2. Anchorage of ties

In the STM, reinforcing bars are assumed to be able to develop their full tensile strength and have a constant force over the length of the tie. Hence, full anchorage of a reinforcing bar is necessary to assume yield will occur. If an insufficient bond length is provided, the tie can't develop its full capacity and a limit should be applied to the maximum force that can be taken by the tie. Clark [35] suggests an ultimate limit should be applied to the assessment force of a bar $F_{n,tie,ult}$ of:

$$F_{n,tie,ult} = \frac{\alpha\beta}{\gamma_{mb}}\sqrt{f_c}\pi d_b l_a \tag{9}$$

where l_a is the actual provided anchorage length of the bar (which is less than the full anchorage length), α is the residual bond strength factor in the range of 0.15–0.40, β is the bar type coefficient (0.70 in case of deformed bars in tension) and γ_{mb} is a partial safety factor equal to 1.4, unless the worst credible concrete strength is used, in which case it is equal to 1.25.

As an alternative approach to the more rigorous method described above, a reduction factor λ can be applied to all the tension ties within a strut-and-tie model based on their anchorage conditions [35]. The factor λ is calculated as the ratio of the actual bond length to the required anchorage length (if sufficient anchorage is provided, λ is taken as equal to 1.0). It is emphasised that this method does not strictly satisfy the requirements of a lower bound method, but does provide a simplified approach.

3.3. Concrete cracking

Little to no guidance is provided by codes and standards on how to account for cracking in the assessment of structures by means of strut-and-tie methods. Minor crack formation is indirectly taken into account in STMs by means of the effective stress levels. In zones where tensile stresses (and hence cracks) might develop, the allowable effective stress of the strut is reduced, as discussed in Section 2.3.1. However, this does not cover all the types of cracks that can occur in reinforced concrete half-joints where, for example, deterioration has led to additional cracks.

Mander and Scott [43] studied alkali-silica reaction (ASR) and delayed ettringite formation (DEF) in beams and developed an appropriate strut-and-tie method. The expansive nature of the ASR/DEF process was modelled and the confining action of reinforcement and compressive forces in the struts accounted for. This resulted in forces reflecting the ASR/DEF expansion strains being introduced into the STM at the nodes.

One of the major causes of concrete cracking in existing structures is, however, corrosion. Due to the formation of expansive corrosion products at the surface of the reinforcing bars, longitudinal cracks along the bars might develop. As this phenomenon is rarely addressed in STM related documents, there is little guidance for assessors to account for longitudinal cracks in their assessments. However, research on bond capacities of corroded reinforcing bars has proven anchorage capacities can be significantly reduced due to crack formation [44].

Desnerck et al. studied the effect of cracks on the bond behaviour of reinforcing bars subjected to different levels of confinement [45]. The results showed a reduction of the bond capacity as high as 65% in some cases. A potential method to take this reduction into account in STM assessments, is by applying a bond factor α_{cr} to the bond strength of the concrete:

$$f_{bd,red} = \alpha_{cr} f_{bd} \tag{10}$$

where $f_{bd,red}$ is the reduced bond strength and f_{bd} is the design bond strength (assuming perfect bond conditions). For direct pull-out specimens considered in [45], the bond factor α_{cr} was found to be 0.85 for highly confined bars with a single crack or 0.70 in the case of double cracked regions. The corresponding values were 0.40 and 0.30 for unconfined single and double cracked specimens respectively [45]. Further work needs to be done to determine reduction factors for other scenarios, and evaluate the applicability of these factors to RC half-joint beams.

Despite the fact that there is recognition that concrete cracking can significantly reduce the anchorage capacity of reinforcing bars in concrete [44,45], the potential impact of concrete cover spalling has not been quantified for half-joint structures, e.g. in [9].

In order to gather insight in the effect of improper anchorage, concrete cracking in the anchorage zone and changes in the reinforcement layout on the load carrying capacity of reinforced concrete half-joints, a large-scale half-joint experimental program was undertaken. The results of the study are used to help evaluate the accuracy of the STM and the potential for modifying the STM to reflect deterioration processes.

4. Experimental program

In the experimental program, different anchorage, reinforcement layouts, concrete quality and anchorage zone cracking conditions (a total of 12 scenarios) were tested and analysed. A total of six beams each with two half-joint ends were cast. Further details can be found in [46].

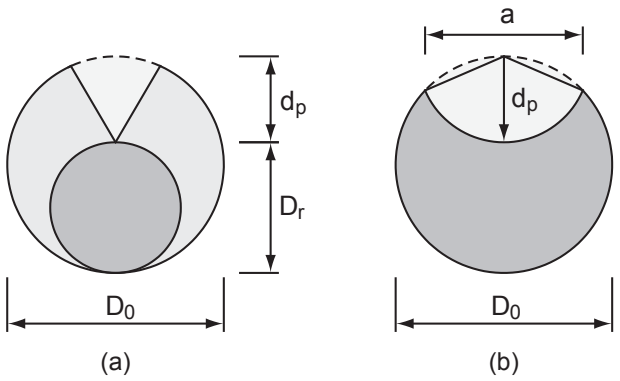

Fig. 9. Residual cross-section after pitting corrosion according to (a) Rodriguez [37] and (b) Val and Melchers [38].

4.1. Test setup and scenarios

The half-joint beams had an overall height of 700 mm and a reduced height at the nib of 325 mm, a length of 3320 mm and a thickness of 400 mm. The beams were cast using a normal strength (C30/37) or low strength (C12/15) concrete according to European strength classes [31] with a maximum aggregate size of 10 mm. After curing for 72 h, the specimens were stored in a standard lab environment (21 ± 2 °C and a relative humidity of 70 ± 10% as measured by a relative humidity/temperature sensor) until the date of testing (27–35 days).

A reference half-joint was designed according to STM principles and is shown in Fig. 10. The bottom reinforcement consisted of 5 bars with a diameter of 25 mm, 5 bars of diameter 20 mm were used as top reinforcement and the shear reinforcement consisted of two-legged stirrups with a diameter of 10 mm in the D-region, while three-legged stirrups with a diameter of 10 mm were used in the B-region (over-reinforced to avoid premature shear failure in the central section of the beam). In the nib, 4 diagonal reinforcing bars with a diameter of 12 mm were placed, as well as 3 U-shaped reinforcing bars with a diameter of 12 mm. The anchorage length of the individual bars (especially the U-bars and diagonal bars) are also indicated in Fig. 10. All reinforcement bars were ribbed and their mechanical properties are given in Table 3.

The beams were tested in three-point bending under a stepwise increasing central load until failure at one half-joint end occurred. The specimens were then unloaded, the support at the failed end moved inwards, and the loading restarted until failure occurred at the opposite end as well. During the test, the applied load, deformations, strains in the reinforcing bars at multiple locations and crack pattern were recorded. More information about the applied test setup, casting process and instrumentation can be found elsewhere [46].

An overview of the different parameter combinations is given in Table 4 indicating the aspects incorporated into the different specimens [46,47]. As a first step, a series of specimens were designed to evaluate the impact of changes in the reinforcement layout and omittance of certain reinforcing bars. As such, a reference specimen (NS-REF), a specimen without diagonal bars (NS-ND), without U-Bars (NS-NU) and with a reduced number of shear links (NS-RS) were tested.

In specimen NS-AD, the anchorage of the diagonal bars was reduced by removing the hooked anchorage. The cross-sectional area of the bars in the inner nib region (see Fig. 10) were reduced by 50% in specimen NS-LR to mimic localised corrosion. This was achieved by locally milling down the bars as will be discussed in a later section.

The impact of anchorage cracking was evaluated using specimens NS-CC&AL (locally cracked concrete around the ends of the bottom reinforcement) and NS-PS&AL (local insertion of a plastic sheet at the ends of the bottom reinforcement) as shown in Fig. 11. In both cases, only 2 tensile reinforcing bars were provided over the full length of the specimen, whereas the remaining three bars were curtailed at their intersection with the diagonal bar. In specimen NS-CC&AL, two sets of three cracked cylinders with a length of 110 mm were placed around the longitudinal bottom reinforcement bars anchorage zone, with a spacing of 10 mm to allow for the placement of the stirrups. The plastic sheet applied in specimen NS-PS&AL, was placed in the same zone as the cracked cylinders were placed for NS-CC&AL (last 340 mm of the reinforcing bar).

In the final test series, the impact of a lower concrete compressive strength (15.4 MPa at the age of testing) and synergistic effects was simulated. A lower concrete strength reference specimen (LS-REF), and a specimen with a combination of reduced shear reinforcement and the curtailment of the bottom bars, LS-AB&RS&AL, were tested. Specimen NS-PS&AD&AL combined the insertion of a plastic sheet at the anchorage zone of the bottom reinforcement with improper anchorage of the diagonal bar, while specimen LS-PS&AD&RS&AL further reduced the capacity by also reducing the concrete strength.

All the test specimens are schematically shown in Fig. 12.

Table 3
Mechanical characteristics of the reinforcing bars.

ϕ [mm]	f_y [MPa]	f_u [MPa]
10	539	596
12	529	559
25	578	674

4.2. Test results

The maximum load applied to the specimens (considered to be the failure load F_{ult}) was recorded for all the beams and is reported in Table 5. Both reference specimens obtained a failure load of over 400 kN even though a weaker concrete was used in LS-REF than in NS-REF, indicating that for the given reinforcement layout the concrete strength was not governing the failure. The impact of reducing the amount of shear reinforcement to about 50% in the D-region or the introduction of cracks around the bottom reinforcement (by means of cracked cylinders or plastic sheets) seemed to have a small impact on the load carrying capacity. When the diagonal bars or U-bars were not placed, or when a local reduction of the reinforcing bar diameters at the

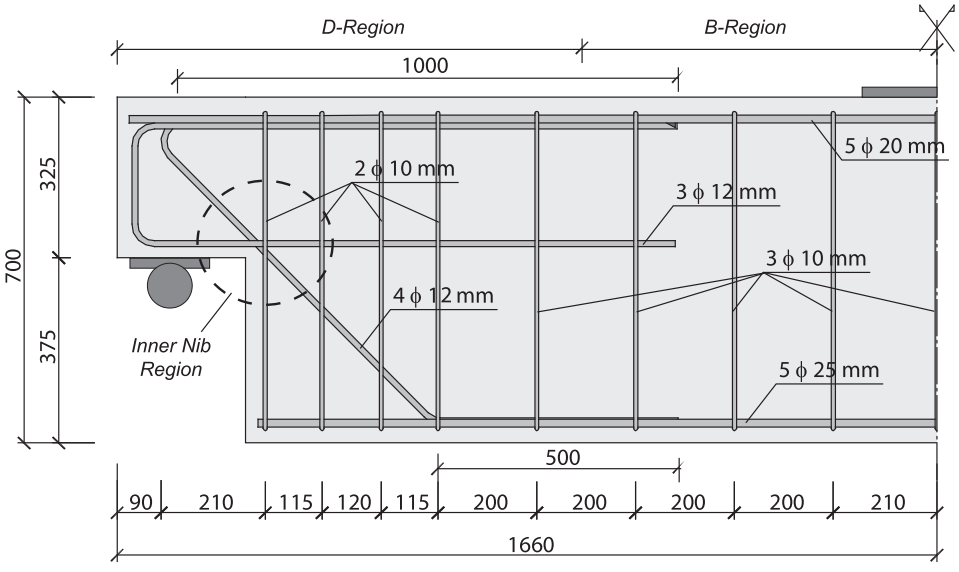

Fig. 10. Geometry and dimensions of experimental half-joint specimens NS-REF and LS-REF.

Table 4
Specifications of different tested reinforced concrete half-joints.

Specimen	Concrete strength		Omitted or reduced area				Anchorage		Cracking	
	C12/15	C30/37	Diagn. bars	U-bars	Stirrups	Local reduct.	Diagn. bars	Bottom bars	Cracked cylinder	Plastic sheet
NS-REF		X								
NS-ND		X	X							
NS-NU		X		X						
NS-RS		X			X					
NS-LR		X				X				
NS-AD		X					X			
NS-CC&AL		X						X	X	
NS-PS&AL		X						X		X
LS-REF	X									
LS-AB&RS&AL	X				X			X		
LS-PS&AD&AL	X						X	X		X
LS-PS&AD&RS&AL	X				X			X		X

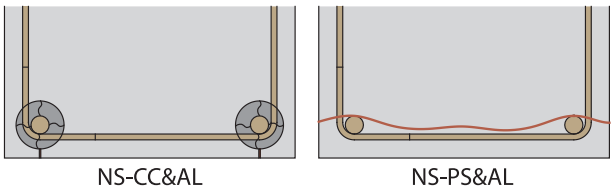

Fig. 11. Induced anchorage cracking for specimens NS-CC&AL and NS-PS&AL.

inner nib zone was applied, the loss in the load carrying capacity was around 40% relative to the original capacity of the equivalent reference beam.

Synergistic effects occurred when several defects were combined, leading to a strength reduction of more than 55% in the worst case scenario (LS-PS&AD&RS&AL).

5. STM predictions of load carrying capacity

For all the 12 experimentally tested half-joints, a statically determinate STM was developed according to the principles discussed in Sections 2 and 3, and based on the actual reinforcement layout and deterioration state. In order to be able to compare the obtained STM failure load predictions with the experimentally obtained results, all load factors and material safety factors were set to unity. The STM tie forces were compared to the experimentally measured reinforcing steel stresses recorded by means of strain gauges. In this way, the impact of various parameters on the failure loads predicted by the STM, $F_{ult,STM}$, can be analysed. The comparisons were performed using the mean value of the recorded stresses since strain gauges were mounted to the reinforcing bars closest to the concrete outer surface on both sides of the specimen. Stresses measured at a specific location in the specimen were considered to be representative of the stress in the tie in the corresponding STM model. Special care was taken when strain gauges were located close to cracks to assure the measurements reflected the overall bar stresses rather than local phenomena linked to the crack formation.

Table 6 provides a comparison of the experimentally recorded failure loads of the specimens and the STM predictions.

For all the specimens, the predicted load carrying capacity from the STM was governed by the yielding of the reinforcing bars (under-reinforced half-joint) or insufficient anchorage lengths, rather than exceeding the capacity of the concrete struts. This was the case even for the lower concrete strength specimens. The longitudinal reinforcing steel bars had a diameter of 25 mm which, even according to AASHTO principles, allowed for the use of the full width (minus the concrete cover layer as indicated in Fig. 4) of the specimen in the STM. For all the beams, the five possible STM combinations shown in Fig. 3 were considered, and the location of the nodes was optimised based on the reinforcement layout, the allowable stresses in the concrete struts/nodes as per EC2 provisions and the force redistribution in the different bars. The STM leading to the highest lower bound was selected.

With respect to criteria used for evaluating the capacity of the compressive struts, all the approaches detailed in Table 2 were considered. No concrete ties were used (given the concerns raised earlier).

The impact of the different parameters on the STM predictions and the corresponding experimental results are discussed in detail in the following.

5.1. Influence of the compressive strength

The strut-and-tie model for NS-REF is shown in Fig. 13. The model consists of ties along the bottom longitudinal bars, along the U-bars and along the diagonal bars. Additional ties are provided by the stirrups (the first and second stirrup were grouped in the STM – an assumption which was verified during the nodal checks). Compressive struts are positioned along the top reinforcement, in the nib, and in the full depth section, completing a combination type model as shown in Fig. 3e.

The position of the deflection point B on the diagonal bar and the location of the node C at the top of the first vertical tie (representing the first and second stirrup) were determined by an iterative process to take full advantage of the provided reinforcement. By repositioning the nodes, the load distribution in the diagonal bar and the stirrups can be altered to achieve the highest failure load. The strut-and-tie model predicts that the half-joint should have a load carrying capacity $F_{ult,STM}$ of 336.5 kN when the strut AB makes an angle of 67.6° with the horizontal and the strut BC is at an angle of 28.5°.

At the predicted STM failure load of 336.5 kN, the diagonal tie as well as the first stirrups reach their yield strength almost simultaneously (the measured reinforcing steel stresses in the diagonal bars and the first stirrup at a load of 336.5 kN were 533 MPa and 494 MPa respectively). The required bar force F_{FG} of 134.8 kN could be properly anchored with the five bars with a diameter of 25 mm over the provided anchorage length. However, whereas the strut-and-tie model predicts stresses in the U-bars of 406 MPa, experimental data shows that these bars were yielding as well. A potential explanation might be that in the actual test, the positions of the struts are not fixed in time and hence might rotate as soon as certain bars are yielding in order to redistribute forces and develop higher load carrying capacities. This hypothesis is supported by the observed crack pattern. Cracks initially formed in the nib at an angle of 60° with the horizontal at load levels of about 200 kN, whereas at a higher load level of 300 kN, cracks formed at an angle of 45° as shown in Fig. 14.

The comparison with the actual experimental data shows that the STM provides a safe underestimation of the load carrying capacity (the actual failure load $F_{ult,exp}$ was 402 kN) which is expected from a plasticity-based lower bound method. The STM underestimates the actual

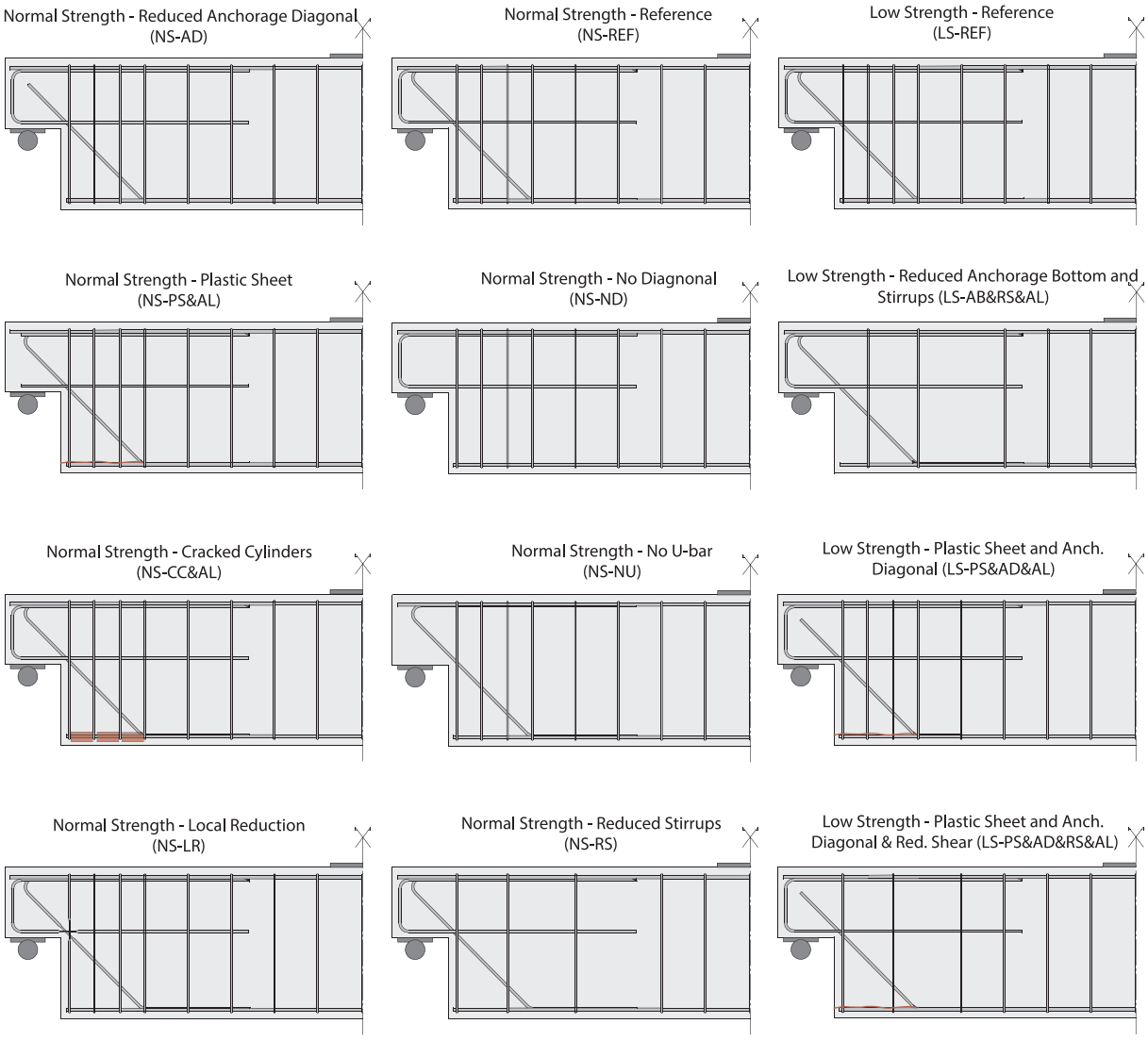

Fig. 12. Reinforcement layouts of the different tested half-joints.

Table 5
Specifications for the different tested reinforced concrete half-joints.

Specimen	F_{ult} [kN]	Failure mode
NS-REF	402.3	Rupture of bars at inner nib zone
NS-ND	244.9	Rupture of diagonals bars and first stirrup
NS-NU	295.8	Rupture of U-bars and first stirrup
NS-RS	358.7	Shear failure with crack originating at bottom corner
NS-LR	261.9	Rupture of bars at inner nib zone
NS-AD	394.6	Shear failure combined with spalling and debonding of bottom bars
NS-CC&AL	367.6	Anchorage failure bottom reinforcement
NS-PS&AL	385.0	Anchorage failure bottom reinforcement
LS-REF	400.0	Rupture of bars at inner nib zone
LS-RS&AL	302.8	Shear failure combined with spalling and debonding of bottom bars
LS-PS&AD&AL	234.9	Anchorage failure bottom reinforcement
LS-PS&AD&RS&AL	177.1	Anchorage failure bottom reinforcement

failure load by about 16%.

A similar strut-and-tie model can be developed for specimen LS-REF, which was cast with a lower grade concrete. Due to the lower compressive strength, the anchorage lengths are increased, however, the provided anchorage length for the bottom reinforcement still suffices. Therefore, the same failure load as for NS-REF is predicted by the STM.

The experiments confirmed that the concrete strength was not critical, and the specimen failed at a load of 400 kN. The critical components once again were shown to be the diagonal tie and first stirrups and a similar crack rotation was noted. The initial cracks appeared at an angle of 60°, while cracks occurring at higher loads formed at an angle of 47°.

5.2. Influence of the reinforcement layout

The impact of the reinforcement layout was investigated by comparing specimens NS-NU, NS-ND, and NS-RS.

When no U-bars are provided, the combination type STM can no longer develop. In this specimen, the external forces exerted by the supports are carried to the top of the nib by a compressive strut and from that point they are transferred to the full depth section by means of a tension tie along the diagonal reinforcement bars and a compressive strut at the top of the specimen (diagonal type STM as shown in Fig. 3a). In diagonal type strut-and-tie models, the assessor has limited possibilities for optimising the load sharing between the different components. The position of node B (Fig. 15) is determined by the location where the compressive strut AB and the diagonal reinforcing tie meet.

Table 6
Comparison of experimental and STM failure loads.

Specimen	$F_{ult,exp}$ [kN]	$F_{ult,STM}$ [kN]	$F_{ult,STM}/F_{ult,exp}$ [%]	Controlling element in STM
NS-REF	402.3	336.5	83.6%	Yielding of diagn. bars and first stirrup
NS-ND	244.9	149.0	60.8%	Yielding of U-bars and first stirrup
NS-NU	295.8	207.0	70.0%	Yielding of diagonal bars
NS-RS	358.7	261.0	72.8%	Yielding of diagn. bars and stirrups
NS-LR	261.9	187.0	71.4%	Yielding of diagn. bars and U-bars
NS-AD	394.6	181.0	45.9%	Anchorage of diagonal bar
NS-CC&AL	367.6	288.5	78.4%	Anchorage of longitudinal bars
NS-PS&AL	385.0	312.0	81.0%	Anchorage of longitudinal bars
LS-REF	400.0	336.5	84.1%	Yielding of diagn. bars and first stirrup
LS-RS&AL	302.8	246.0	81.2%	Yielding of diagn. bars and first stirrup
LS-PS&AD&AL	234.9	113.0	48.1%	Anchorage of diagonal and long. bars
LS-PS&AD&RS&AL	177.1	76.0	42.9%	Anchorage of diagn. bars and yielding 1st stirrup

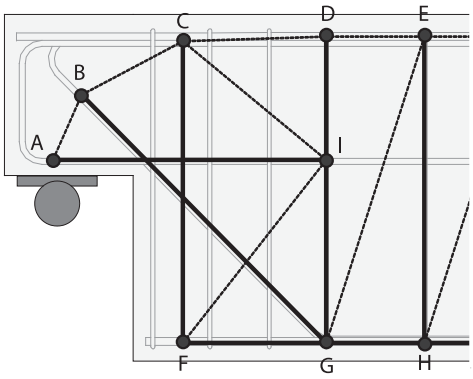

Fig. 13. Strut-and-tie model for specimens NS-REF and LS-REF.

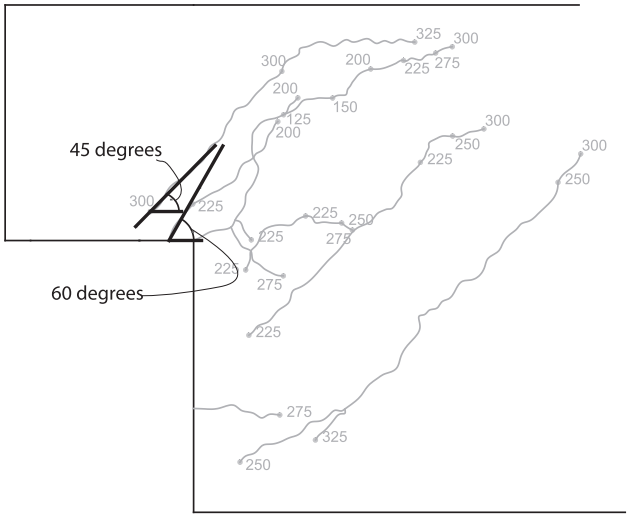

Fig. 14. Crack formation and crack angle in the nib of specimen NS-REF.

As shown in Fig. 15, the first four stirrups do not contribute to the truss and hence the obtained failure load is significantly lower than for the reference specimen. The ultimate failure load predicted by the STM, $F_{ult,STM}$, was found to be 207.0 kN at which point yielding of the diagonal reinforcing bar is induced.

The actual recorded failure load of the specimen, $F_{ult,exp}$, was 295.8 kN indicating the STM model underestimated the failure load by about 30%. The recorded stresses in the diagonal bars were 448 MPa at a load level of 207 kN, which were lower than the yield stress predicted by the STM at this load level. During the experiments yielding of the diagonal bars was noted at 250 kN. Experimental data also showed significant stresses being built up in the first stirrup. At a load of 207 kN (the STM predicted failure load), the steel stresses in the first stirrup are

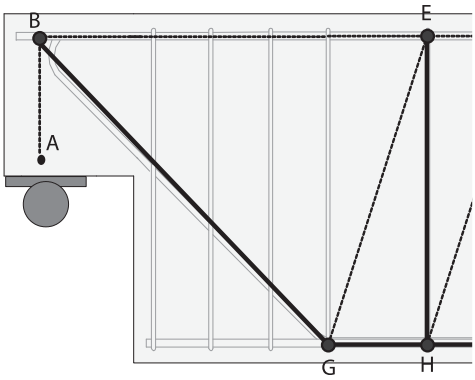

Fig. 15. Strut-and-tie model for specimen NS-NU.

around 260 MPa. The subsequent stirrups carry little or no load and the measured steel stresses are below 20 MPa. This seems to indicate that, although the crack pattern confirms the verticality of strut AB [46], a load path is being developed in the specimen where the first stirrup is activated as a tie.

When no diagonal bar is present (specimen NS-ND), neither a combination type STM nor a diagonal type STM can develop. Fig. 16 shows the orthogonal STM mapped onto the reinforcement layout of specimen NS-ND. The location of node C was varied in order to influence the load sharing between the different ties that line up with the stirrups and the U-bar. Failure in the STM was reached at a load of 149.0 kN and was governed by the yielding of the U-bars as well as the first stirrup.

The actual failure load of 244.9 kN for specimen NS-ND was significantly higher than the calculated $F_{ult,STM}$ of 149.0 kN, leading to an underestimation of the failure load by the STM of 39%. The failure mode is predicted correctly in that the experimental specimen failed

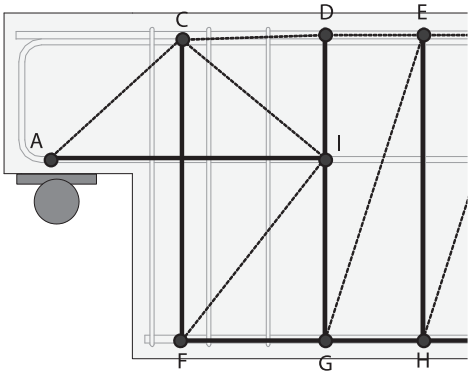

Fig. 16. Strut-and-tie model for specimen NS-ND.

due to the yielding (and rupture) of the U-bars and first stirrup. However, the experimentally determined load at which the first stirrup started to yield was 200.8 kN, whereas the U-bars started to yield at a load of 216 kN. The possibility of the existence of a concrete tie at the location of the missing diagonal bar is unlikely. The crack initiated at the inner nib of the specimen and had grown significantly by the time a load level of 125 kN was reached, cutting the entire zone in which a concrete tie could develop.

Reducing the amount of shear reinforcement had a significant impact on the predicted failure load. The combination type STM for NS-RS shows high similarities with the one for NS-REF. Due to the reduced amount of stirrups, however, the location of the ties was adjusted and the tie capacity significantly reduced. In this way, a predicted failure load of 261 kN was obtained at which point the first stirrup, second stirrup as well as diagonal bars were predicted to yield simultaneously. The calculated stresses in the U-bar at this point were only 150 MPa.

The experimental results confirmed the failure to be due to the yielding of the first stirrup and diagonal bar, but at a much higher load level of 358.7 kN. At this point, the U-bars were close to yielding as well, which is not reflected in the STM.

5.3. Influence of detailing

The impact of a reduced anchorage length due to improper detailing is taken into account in strut-and-tie models at the level of the nodal checks where the capacities of the ties are reduced based on the available anchorage length (see Section 3.2).

For specimen NS-AD, the maximum load carrying capacity as determined by the STM is governed by the anchorage capacity of the diagonal bar at the lower end of the bar (the STM model as shown in Fig. 13 was applied). Due to the limited anchorage length (in this specimen the bend and extension of the bar along the bottom reinforcement was not provided), only a limited force can be developed in the diagonal bar (see Fig. 17). This results in a failure load for NS-AD of 181 kN which represents a slight increase in $F_{ult,STM}$ of 32 kN when compared to NS-ND, a case where the diagonal bar was not present. It has to be noted that the allowable force in the diagonal tie of 41.1 kN was determined using the simplified method (ratio of provided to required bond length) as proposed by Clark [35] using the EuroCode 2 provisions [31] for calculating the required anchorage length and setting all safety factors to 1.0. When the more elaborate approach, using Eq. (9) is used, a lower allowable tie force is obtained, reducing $F_{ult,STM}$ to 170.5 kN.

The tested specimen NS-AD failed at 394.6 kN which is a much higher load than the STM prediction. The beam exhibited a shear failure and debonding of the bottom reinforcing bars (which was initiated by the debonding of the diagonal reinforcement).

The discrepancy between the STM predictions and the experimentally determined failure load can possibly be explained using the measurements of the steel stresses in the diagonal reinforcing bars. Whereas the EuroCode 2 (without applying safety factors) accounts for a bond strength of 5.1 MPa for the ribbed reinforcing bars and concrete compressive strength used in the current work, the experimentally measured steel stresses indicate much higher bond stresses. At the moment of failure (394.6 kN), the strain gauges recorded a reinforcing steel stress of 160 MPa in the diagonal bars at a distance of 20 mm from the end of the bar. Assuming a uniform stress distribution over the anchorage length of the bar, this results in an average bond stress of 24 MPa. This value is in line with experimentally determined pull-out bond strengths for similar bar diameters and concrete strengths [45,48]. When a bond strength of 24 MPa is applied in the STM, the ultimate failure load increases significantly to 300.5 kN at which point anchorage failure of the diagonal bar occurs simultaneously with yielding of the first stirrup and U-bars. Although applying a higher bond strength of 24 MPa leads to an improvement in the predicted failure load, special care needs to be taken when other reinforcement layout, concrete strengths and/or confinement conditions are considered. Applying bond strength values as provided by the standards and guidelines will, in most cases, provide a safe lower limit to the actual failure load.

5.4. Influence of deterioration

The impact of deterioration outcomes were investigated in the experimental program in two ways. In specimen (NS-LR), a local reduction of the steel bar diameters at the nib were used to mimic local corrosion in the nib reinforcement, while in specimens NS-PS&AL and NS-CC&AL the impact of crack formation in the anchorage zone of the longitudinal reinforcement was studied. In practice longitudinal cracks could form due to expansive forces generated in the concrete due to steel corrosion.

A combination type model similar to that of NS-REF (see Fig. 13) was found to be relevant for specimen NS-LR. The location of the ties and struts were unchanged, however, the capacity of the diagonal bars, U-bars, and first stirrup were reduced. Despite the fact that only a central part of the rebars was milled down to 50% of their original section in the STM, the capacity of the entire tie was reduced accordingly. The STM predicted failure load turned out to be 187.0 kN with the critical elements being the diagonal bars and U-bars that simultaneously reached their yield capacity.

The yielding of the diagonal bars and U-bars was confirmed in the experiments, and shortly after the yielding of these bars, the first stirrup started to yield as well. The specimen finally failed due to the rupture of all the bars in the inner corner of the nib at a failure load of 261.9 kN, which means the STM model prediction was 71.4% of the actual failure load.

With respect to the specimens NS-PS&AL and NS-CC&AL, the current codes and standards do not provide any guidance on how to deal with cracks in the anchorage zone. Hence, applying standard strut-and-tie methods (and a combination type STM as in Fig. 13) would lead to similar capacities for reference specimens as for the specimen with induced cracks along the bottom reinforcement. When the longitudinal cracks are taken into account, according to the principles described in Section 3.3, $F_{ult,STM}$ would expect to be reduced. In the case of NS-CC&AL, a confined state of double cracking exists in the anchorage zone of the longitudinal bottom bars. Whereas in the case of NS-PS&AL the situation is more analogous to a confined single cracked anchorage zone. In both specimens, the confinement is provided by the shear stirrups crossing the crack planes in the anchorage zone. The ultimate loading capacity in both cases is limited by the anchorage capacity of

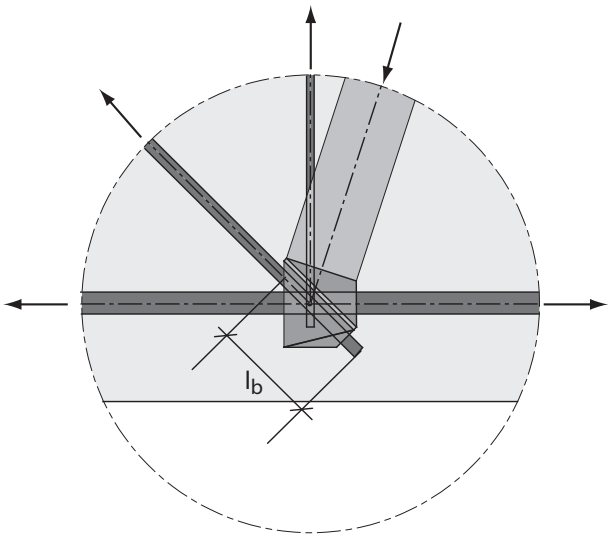

Fig. 17. Provided anchorage length of diagonal reinforcement assuming a hydrostatic nodal zone.

the longitudinal reinforcement and hence the force that can build up in the tie FG (see Fig. 13). For specimen NS-PS&AL a predicted failure load of 312.0 kN is obtained, while NS-CC&AL has a lower $F_{ult,STM}$ of 288.5 kN due to a higher penalty for double cracked anchorage zones. However, it has to be emphasized that the bottom reinforcing bars are well confined by the stirrups and, hence, the bond properties of half-joint structures with reduced confinement or with alternative geometries/reinforcement lay-outs might differ siginificantly. Further research needs to be done to develop a specific methodology to account for anchorage zone cracking.

The experimental results confirm that the strength capacity of NS-CC&AL was lower than that of NS-PS&AL. Both specimens failed due to the debonding of the longitudinal reinforcement. The failure loads were 367.6 kN and 385.0 kN respectively or 27.4% and 23.4% higher than the predicted values. The maximum force that was built up in section FG along the longitudinal reinforcement during the experiments was 185.6 kN for NS-PS&AL and 167.0 kN for NS-CC&AL. Comparing these numbers to the STM tie capacity limits of 114.5 kN and 92.5 kN, shows that the actual forces in the reinforcement were higher than calculated by the STM. This is most likely due to the high confinement provided by the stirrups in the anchorage zone.

5.5. Synergistic effects

The impact of changes in the concrete compressive strength on the STM assessment was small as shown in Section 5.1. However, when the compressive strength reduction was combined with a reduction in the amount of the reinforcing bars in the anchorage zone and reduced shear reinforcement (specimen LS-RS&AL), the impact of the compressive strength was reflected in a decrease in the bond strength. Due to this decrease in cube compressive strength, $f_{c,cub}$, from 35.8 MPa to 15.2 MPa, the required anchorage lengths increased by 75.5%. Given the fact that in reducing the amount of shear reinforcement the first and third stirrup were removed, the first vertical tie in the STM (tie CF in Fig. 13) is shifted inwards as well, resulting in an increased available bond length for tie FG. Hence, the anchorage of the bars turns out not to be critical in the STM assessment, and the capacity of the beam is limited by the yield strength of the diagonal bars and the shear reinforcement. An assessed ultimate failure load of 246 kN was obtained which is 81.2% of the experimental value of 302.8 kN.

The predicted failure load drops to 113 kN when, in addition, the diagonal bars are improperly anchored (specimen LS-PS&AD&AL). In the STM assessment, both the anchorage of the diagonal bar as well as the anchorage of the bottom reinforcement become critical. Whereas some redistribution of forces was possible in specimen NS-AD, resulting in higher demands on the stirrups and bottom longitudinal reinforcement, this is no longer possible when the anchorage of both bars is reduced as is the case in LS-PS&AD&AL.

The experimental results indeed showed that the failure appeared to be induced by the debonding of the longitudinal reinforcement, but at a failure load of 234.9 kN which is significantly higher than the predicted load. However, as was the case for NS-AD, the STM model potentially underestimated the anchorage capacity and hence the force developed in the diagonal tie. Experiments indicated a maximum diagonal bar force of 56.2 kN while the STM model only allows for a force of 21 kN, confirming the earlier observation that the high confinement at node G (Fig. 13) allows for the development of higher bond stresses than given by the EuroCode 2 provisions.

A similar conclusion can be drawn for LS-PS&AD&RS&AL. By reducing the amount of shear reinforcement, in addition to the lower compressive strength and improper anchorage of the diagonal and longitudinal bars, the capacity decreases to 72.5 kN according to a combination type STM model. The experimentally obtained value, however, is 177.1 kN, indicating an underestimation of more than 100%. In contrast to LS-PS&AD&AL, the STM capacity of LS-PS&RS&AD &AL is governed by the anchorage of the diagonal bar and the yield strength of the shear reinforcement. A redistribution of forces from the diagonal bars to the stirrups and longitudinal reinforcement is no longer possible due to the low amount of shear reinforcement provided.

6. Conclusions

The design of disturbed regions in reinforced concrete half-joints is traditionally performed by means of strut-and-tie modelling. A truss consisting of struts and ties is assumed as a system to transfer the forces through the D-region into the B-region. The design provisions found in standards and codes can be used for the assessment of existing structures with minor adjustments. However, current documents provide limited guidance on the incorporation of deterioration aspects such as corrosion, insufficient anchorage lengths, and crack formation. To reflect corrosion, a reduction in the cross-sectional area of the reinforcing bar, and thereby the capacity of the tension tie, can be incorporated. Insufficient anchorage lengths can be taken into account using a proportional reduction in the tie capacity or by penalising the residual bond capacity. In this paper, suggestions have been made to allow assessors to incorporate longitudinal crack formation into the capacity checks. It is suggested to reduce the bond strength of the concrete by a factor ranging from 0.85 to 0.3 depending on the confinement conditions and the crack state. In some cases, the reduction factor can even be as low as 0.0.

Experiments performed on 12 half-joint beams demonstrated the effects of single defects. Synergistic effects also exist and might lead to much higher reductions than expected from the sum of individual defects.

For the beams studied in the current work, the governing conditions in the STM assessments turned out to be the capacity and the anchorage conditions of the ties. In all cases, the STM predictions were lower than the experimentally obtained capacity, as would be expected from a lower bound method. However, the underestimation varied significantly within a range of 57–16%. A lack of anchorage capacity in the diagonal bar seemed to be penalised significantly by the STM where experimental results indicated a lower reduction in capacity, indicating further research into the anchorage of ties in highly confined nodes is necessary.

When cracks are present in the anchorage zone, those should not be disregarded, as current standards and guidelines seem to indicate. Their impact on the load carrying capacity was clearly noted during the experimental program. Based on pull-out tests performed on reinforcing bars embedded in cracked concrete, an approach applying reduction factors to the bond strength is proposed. This reduction factor would vary depending on the crack state and the extent of cracking. Further research is needed to obtain sufficient data to develop a rigorous method applicable for half-joints with geometries, reinforcement lay-outs and confinement different from the ones applied in this study.

Based on this study, it can be stated that current codes and standards, combined with recent findings and guidelines on deterioration effects, led to safe load bearing capacity estimates for a specific set of experimentally tested reinforced concrete half-joints. However, the developed STMs seem to be, in some instances, unable to pick up alternative load paths that develop as soon as the capacity of a certain tie is reached. Hence the actual capacities might be higher than what is obtained from STM calculations, however, a wide range of obtained $F_{ult,exp}/F_{ult,STM}$ ratios is obtained indicating assessors should treat the results with due care.

Acknowledgements

The authors would like to acknowledge the financial support of EPSRC – the Engineering and Physical Sciences Research Council (UK) – through the EPSRC Project ‘Reinforced concrete half-joint structures: Structural integrity implications of reinforcement detailing and deterioration’ [Grant no. EP/K016148/1].

Additional data related to this publication is available at the University of Cambridge's institutional data repository: https://doi.org/10.17863/CAM.18300.

References

[1] Johnson P, Couture A, Nicolet R. Commission of inquiry into the collapse of a portion of the de la Concorde overpass – report; 2007.
[2] Mattock A, Chan T. Design and behavior of dapped-end beams. PCI J 1979:28–45.
[3] Allison B. The structures management information system (SMIS) database. Bridg. Manag. 5 Insp. maintenance, Assess. repair; 1999.
[4] Desnerck P, Lees JM, Morley CT. Assessment of reinforced concrete half-joint structures: dealing with deterioration. In: Proc. 2014 PCI conv. natl. bridg. conf., Washington DC, USA: Precast/Prestressed Concrete Institute; 2014. p. 16.
[5] Mitchell D, Marchand J, Croteau P, Cook W. Concorde overpass collapse: structural aspects. J Perform Constr Facil 2011;25:545–53.
[6] ACI Committee 318. Building code requirements for reinforced concrete (ACI 318-56). Detroit; 1956.
[7] Mitchell D, Cook W, Peng T. Importance of reinforcement detailing. ACI Spec Publ 2010;273:1–16.
[8] Prestressed Concrete Institute. PCI design handbook. 7th ed. Precast/Prestressed Concrete Institute; 2007.
[9] Loudon N. IAN 53/04 – concrete half-joint deck structures; 2004. p. 18.
[10] Department of Transportation. BA39/93 assessment of reinforced concrete half-joints; 1993. p. 22.
[11] fib Task Group 4.4. fib Bulletin 45 – practitioners' guide to finite element modelling of reinforced concrete structures. Lausanne, Switzerland: International Federation for Structural Concrete (fib); 2008.
[12] BSI. PD 6687-1:2010 Background Paper to the National Annexes to BS EN 1992-1 and BS EN 1992-3. London, UK: British Standards Institution (BSI); 2010.
[13] Schlaich J, Schafer K, Jennewein M. Towards a consistent design of structural concrete. PCI J 1987:77–150.
[14] Narayanan R. Precast Eurocode 2: design manual. Leicester, UK: British Precast Concrete Federation; 2007.
[15] Goodchild C, Morrison J, Vollum R. Strut-and-tie models. Camberley, UK: The Concrete Centre; 2014.
[16] European Committee for Standardization. EN 1992-1-1 Eurocode 2: design of concrete structures – Part 1–1: general rules and rules for buildings. European Committee for Standardization; 2004.
[17] Fernández Ruiz M, Muttoni A. On development of suitable stress fields for structural concrete. ACI Struct J 2008:495–502.
[18] Tjhin TN, Kuchma DA. Computer-based tools for design by strut-and-tie method: advances and challenges. ACI Struct J 2002;99:586–94.
[19] Wang Q, Guo Z, Hoogenboom P. Experimental investigation on the shear capacity of RC dapped end beams and design recommendations. Struct Eng Mech 2005;21:221–35. http://dx.doi.org/10.12989/sem.2005.21.2.221.
[20] Bergmeister K, Breen J, Jirsa J, Kreger M. Detailing for structural concrete. Austin; 1993.
[21] Wight J, MacGregor J. Reinforced concrete: mechanics & design. 6th ed. New Jersey, US: Pearson; 2012.
[22] ACI Committee 318. Building code requirements for structural concrete (ACI 318M-14) and commentary (ACI 318RM-14). 1st ed. Farmington Hills, MI, USA: American Concrete Institute; 2014.
[23] AASHTO. LRFD bridge design specifications. 7th ed. American Association of State Highways and Transportation Officials; 2014.
[24] Mitchell D, Collins M. Revision of strut-and-tie provisions in the AASHTO LRFD bridge design specifications – final report. Dorion, Canada; 2013.
[25] Alshegeir A. Analysis and design of disturbed regions with strut-tie models. Purdue University; 1992.
[26] MacGregor J. Reinforced concrete – mechanics and design. 3rd ed. Englewood Cliffs, US: Prentice Hall; 1997.
[27] Yun Y, Ramirez J. Strength of struts and nodes in strut-tie model. J Struct Eng 1996;122:20–9. http://dx.doi.org/10.1061/(ASCE)0733-9445(1996) 122:1(20).
[28] Kupfer H, Hilsdorf H, Rusch H. Behavior of concrete under biaxial stresses. ACI J Proc 1969;66:626–66.
[29] ASCE- ACI committee 445. Recent Approaches to Shear Design of Structural Concrete. J Struct Eng 1998;124:1375–417. http://dx.doi.org/10.1061/(ASCE)0733-9445(2000)%20126:7(856).
[30] Schlaich M, Anagnostou G. Stress fields for nodes of strut-and-tie models. J Struct Eng 1990;116:13–23.
[31] European Committee for Standardization. EN 1992-1-2 Eurocode 2: design of concrete structures – Part 1-2: general rules – structural fire design. European Committee for Standardization; 2008.
[32] Bergmeister K, Breen JE, Jirsa JO. Dimensioning of the nodes and development of reinforcement. IABSE Reports, vol 62, IABSE Colloqium; 1991. p. 551–6.
[33] Orangun C, Jirsa J, Breen J. A reevaluation of test data on development length and splices. TX, USA: Austin; 1975.
[34] Department of Transportation. BA38/98 – assessment of the fatigue life of corroded or damaged reinforcing bars, vol. 16; 1993.
[35] Clark L. IAN53 Half-joint assessment advice – ULS Assessment of half-joints. Highways Agency; 2010.
[36] The Highways Agency. BA 51/95 – the assessment of concrete structures affected by steel corrosion; 1995.
[37] Rodriguez J, Ortega L, Garcia A. Assessment of structural elements with corroded reinforcement. In: Swamy R, editor. Proc. int. conf. corros. corros. prot. steel concr., Sheffield, UK: Sheffield Academic Press; 1994. p. 171–85.
[38] Val D, Stewart M, Melchers R. Effect of reinforcement corrosion on reliability of highway bridges. Eng Struct 1998;20:1010–9. http://dx.doi.org/10.1016/S0141-0296(97)00197-1.
[39] Rodriguez J, Ortega L, Casal J, Diez J. Corrosion of reinforcement and service life of concrete structure. In: Sjostrom C, editor. Proc. 7th Int. conf. durab. build. mater. components, Stockholm, Sweden; 1996. p. 117–26.
[40] Harnisch J, Raupach M. The residual cross section factor as a key parameter for the static evaluation of corroding reinforced concrete structures. Mater Corros 2015;66:829–38.
[41] Darmawan M. Pitting corrosion model for reinforced concrete structures in a chloride environment. Mag Concr Res 2010;62:91–101.
[42] Zhu W, François R. Experimental investigation of the relationships between residual cross-section shapes and the ductility of corroded bars. Constr Build Mater 2014;69:335–45. http://dx.doi.org/10.1016/j.conbuildmat.2014.07.059.
[43] Mander J, Scott R. Guidelines for determining the capacity of D-regions with premature concrete deterioration of ASR/DEF; 2015.
[44] Task Group Bond Models. fib Bulletin 10 – bond of reinforcement in concrete. Lausanne; 2000.
[45] Desnerck P, Lees JM, Morley CT. Bond behaviour of reinforcing bars in cracked concrete. Constr Build Mater 2015;94:126–36.
[46] Desnerck P, Lees JM, Morley CT. Impact of the reinforcement layout on the load capacity of reinforced concrete half-joints. Eng Struct 2016;127:227–39.
[47] Desnerck P, Lees JM, Morley CT. The effect of local reinforcing bar reductions and anchorage zone cracking on the load capacity of RC half-joints. Eng Struct 2017;152:865–77. http://dx.doi.org/10.1016/j.engstruct.2017.09.021.
[48] Desnerck P, De Schutter G, Taerwe L. Bond behaviour of reinforcing bars in self-compacting concrete: experimental determination by using beam tests. Mater Struct 2010;43:53–62. http://dx.doi.org/10.1617/s11527-010-9596-6.